Regeneration of sulfur poisoned Pd-Pt/CeO$_2$-ZrO$_2$-Y$_2$O$_3$-La$_2$O$_3$ and Pd-Pt/Al$_2$O$_3$ methane oxidation catalysts

Patrick Lott [1], Mario Eck [1], Dmitry E. Doronkin [1], Radian Popescu [2], Maria Casapu [1], Jan-Dierk Grunwaldt [1*], Olaf Deutschmann [1*]

[1] Institute for Chemical Technology and Polymer Chemistry (ITCP), Karlsruhe Institute of Technology (KIT), Engesserstr. 20, 76131 Karlsruhe, Germany

[2] Laboratory for Electron Microscopy (LEM), Karlsruhe Institute of Technology (KIT), Kaiserstr. 12, 76131 Karlsruhe, Germany

* Corresponding authors: grunwaldt@kit.edu (J.-D. Grunwaldt), deutschmann@kit.edu (O. Deutschmann)

Abstract

The poisoning of Pd-Pt/Al_2O_3 and Pd-Pt/CeO_2-ZrO_2-Y_2O_3-La_2O_3 methane oxidation catalysts by SO_2 was studied under conditions typical for lean burn gas engines. Regeneration of sulfur-poisoned catalysts was achieved by applying rich conditions at 500 °C and 550 °C. The presence of NO_x resulted in a slower deactivation rate. While Pd-Pt/CeO_2-ZrO_2-Y_2O_3-La_2O_3 showed a superior catalytic activity, durability and regeneration ability over Pd-Pt/Al_2O_3 under NO_x-free reaction conditions, its reactivation by a rich treatment was strongly inhibited if NO_x was present during the aging and regeneration process. *Operando* X-ray absorption spectroscopy (XAS) was used to monitor the evolution of Pd and Pt during poisoning and regeneration, revealing the formation of PdS and metallic Pd during reactivation of Pd-Pt/Al_2O_3, followed by transition to PdO after changing to lean reaction gas mixture. On the other hand, Pd species supported on CeO_2-ZrO_2-Y_2O_3-La_2O_3 could not be reduced by rich treatment and no regeneration occurred.

Keywords

Methane oxidation, Emission control, Sulfur poisoning, Pd-Pt catalyst, Catalyst deactivation, *operando* spectroscopy

1   Introduction

Lean burn natural gas engines can significantly contribute to meet the tightening environmental protection legislation for energy and automobile industry. Besides high fuel efficiency and low pollutant emissions, natural gas engines (NGEs) stand out by remarkably low CO_2 emissions due to the convenient H/C-ratio of natural gas, which consists mainly of CH_4. Despite these advantages, NGEs suffer from methane slip originating from incomplete combustion. Since CH_4 is a significant greenhouse gas, finding an effective catalytic way to convert it into carbon dioxide and water at low temperatures is of utmost importance to keep the engines run with natural gas competitive [1, 2].

Noble metal catalysts based on palladium are reported to be the most effective systems in methane conversion, while the activity and durability can be further increased by addition of small amounts of platinum [3]. However, methane oxidation over Pd-based catalysts is strongly inhibited by the inevitable exhaust gas component water, which is produced even by the reaction itself, leading to considerable deactivation with time on stream [4]. Moreover, methane oxidation catalysts (MOCs) are strongly deactivated by sulfur compounds present in the exhaust stream, typically originating from lubricants, odorants or the fuel itself [5]. These lead to formation of adsorbed sulfur species, surface sulfites/sulfates and bulk sulfation of both, the noble metal particles as well as the support [6]. While the transition of catalytically active Pd/PdO to inactive $PdSO_4$ is claimed to be the main reason for activity loss [7], the poisoning of the support material results in even more severe effects, as the sulfur is stored and can spillover back to the noble metal particles [8]. Although addition of Pt is reported to increase the activity and stability to some extent [9], deactivation of Pd-Pt catalysts occurs with time on stream and therefore regeneration procedures are needed. In this regard, rich conditions have been found very suited for reactivation [10]. However, the sulfur remaining on the support after regeneration at mild temperature conditions will re-poison the catalyst immediately after returning to reaction gas mixture, as recently observed for a Pd/Al_2O_3 catalyst [11].

Catalysts supported on CeO_2-ZrO_2 mixed oxide, on the other hand, show less re-poisoning by spillover that leads to a more sustainable regeneration under rich conditions [12].

The results presented in this study report the crucial role of the gas composition and carrier material on the sulfur poisoning process of MOCs. Pd-Pt/Al_2O_3 and Pd-Pt/CeO_2-ZrO_2-Y_2O_3-La_2O_3 catalysts were poisoned by SO_2 in different gas compositions and, subsequently, regenerative treatments under rich conditions were applied. *Operando* X-ray absorption spectroscopy (XAS) at the Pd K-edge and the Pt L_3-edge was used during the regenerative treatment to clarify the impact of the applied conditions on the noble metal state, as this is considered to be the main factor influencing the activity.

2   Experimental

2.1   Catalyst preparation

Pd-Pt/γ-Al_2O_3 and Pd-Pt/ZrO_2-CeO_2-Y_2O_3-La_2O_3 (referred to as Pd-Pt/CZ in the following, as CeO_2 and ZrO_2 are the dominating species) were prepared by incipient wetness impregnation of the two metal-oxide support materials by using an aqueous solution of tetraamminepalladium(II)nitrate (ChemPUR, 3.3 wt.% aqueous solution) and tetraammineplatinum(II)nitrate (VWR, purity > 99.9 %) as noble metal precursors. Due to its low pore volume (0.39 mL/g), two impregnation steps were necessary for the commercial Y_2O_3-La_2O_3-CeO_2-ZrO_2 mixed oxide (metal weight ratio of 5:5:30:60) with 5 h of drying at room temperature and 1 h at 70 °C in static air between the steps. The noble metal weight ratio of Pd:Pt is 5:1, with a total noble metal loading of about 2.4 wt.% (approx. 2.0 wt.% Pd, 0.4 wt.% Pt, as indicated by the elemental analysis results reported in Table S1) for both catalysts. The entire catalyst synthesis procedure was performed by a robot-controlled preparation unit (Accelerator SLT106 Parallel Synthesizer – SLT CATIMPREG, ChemSpeed Technologies) [13]. After impregnation, both samples were dried for 12 h at 70 °C, mortared and calcined in static air at 550 °C for 5 h.

2.2   Catalyst characterization

N_2 physisorption measurements according to the Brunauer-Emmet-Teller (BET) method for surface area and pore volume determination were performed at – 196 °C using a BELSOPRP Mini II analyzer (MicrotracBEL). To remove adsorbates from the surface, the samples were degassed for 2 h at 300 °C prior to each measurement.

The powder catalysts were characterized by means of X-ray diffraction (XRD) using a Bruker Advance D8 diffractometer with Cu Kα radiation (wavelength λ = 0.154 nm). Each measurement was performed with a step size of 2θ = 0.016 ° (0.51 s/step dwell time) between 20 ° to 90 °.

Particle size and chemical composition were analyzed by high-angle annular dark-field scanning transmission electron microscopy (HAADF-STEM) and energy-dispersive X-ray spectroscopy (EDXS) using the Pd $L_{α1}$ and Pt $L_{α1}$ series, respectively. A FEI OSIRIS ChemiSTEM microscope at 200 kV electron energy equipped with a Bruker Quantax system (XFlash detector) was used to analyze the catalyst powders deposited on a copper grid. The results obtained were evaluated using the FEI software package "TEM imaging and analysis" (TIA), version 4.7 SP3 and the Bruker software package ESPRIT (version 1.9).

2.3   Catalytic tests and *operando* XAS procedure

The catalytic activity tests were conducted in a setup dedicated for testing powder catalyst samples, which was in-house built and controlled via a LabView software tool. Bronkhorst mass flow controllers (MFC) were

used to dose the reaction gases, which were preheated in stainless steel tubes to 130 °C. Water was added by combining a Liquiflow and a controlled evaporator mixer (CEM, Bronkhorst). A sieve fraction of $125 - 250$ µm of 300 mg powdered catalysts were diluted with 700 mg quartz sand and fixed in a quartz glass tubular reactor (inner diameter: 0.8 cm), resulting in a 1.5 cm catalyst bed. The whole reactor was placed in a furnace. Thermocouples located 5 mm upstream and downstream the catalyst were used to record the temperature, while the thermocouple upstream the catalyst bed was used to control the furnace temperature. Reaction products were analyzed by using a FT-IR spectrometer (MultiGas 2030, MKS instruments).

Prior to any catalyst test, the samples were degreened for 1 h at 550 °C in 3200 ppm CH_4, 10 % O_2 in N_2 for 1 h. Subsequently, the catalyst samples were aged for 15 h at 450 °C in two different reaction gas mixtures containing 3200 ppm CH_4, 10 % O_2 and 12 % H_2O, 5 ppm SO_2 in N_2 and in some tests also 120 ppm NO, 30 ppm NO_2. In order to regenerate the catalyst after aging, the sample was heated to 500 °C in rich conditions (without O_2 in the feed) for 1 h and then cooled to 450 °C again, where another 15 h of aging conditions were applied. Then the regeneration and aging cycle was repeated at a regeneration temperature of 550 °C (Fig. S 1). The used gas compositions are summarized in Table 1.

Table 1: Reaction gas mixtures that were used during the reaction protocol. Balancing by N_2.

Gas mixture no. (GM)	Gas mixture and step	Temperature [°C]	CH_4 [ppm]	O_2 [%]	H_2O [%]	NO [ppm]	NO_2 [ppm]	SO_2 [ppm]
1	Degreening	550	3200	10	0	0	0	0
2	SO_2-aging	450	3200	10	12	0	0	5
3	SO_2-aging + NO_x	450	3200	10	12	120	30	5
4	Regeneration	500 or 550	3200	0	12	0	0	5
5	Regeneration + NO_x	500 or 550	3200	0	12	120	30	5

To study the fast changes of the active species occurring during transient conditions, *operando* XAS measurements were performed at the ROCK beamline at the synchrotron SOLEIL (Saint-Aubin, France), which is able to record X-ray absorption spectra at two alternating absorption edges consecutively. Hereby, the Pd K-edge (24 350 eV) was measured with a Si(220) monochromator whereas a Si(111) monochromator was used to obtain data at the Pt L_3-edge (11 564 eV). Both absorption edges were measured in transmission mode. For the *operando* investigations, the catalyst bed was fixed in a quartz capillary microreactor with an outer diameter of 1.5 mm and a wall thickness of 0.02 mm. The reaction gases were dosed with MFCs (Bronkhorst) and an additional saturator was added to dose water. The reactor was heated by a hot air gas b

lower system (GSB-1300, FMB Oxford) [14] and for end-of-pipe analysis a FT-IR spectrometer (MultiGas 2030, MKS instruments) was installed to follow the evolution of reaction gases during the *operando* investigations. To keep the results comparable to the laboratory tests, similar conditions (gas composition, temperature, GHSV) like in the lab bench tests were chosen. However, to better identify the differences induced by the different carriers in the noble metal behavior, a slightly lower temperature of 450 °C was selected for catalyst regeneration during the *operando* XAS study. As this temperature is identical with the poisoning temperature, it was ensured that the fast changes occurring when varying the gas composition can be monitored by means of XAS. The obtained data were evaluated quantitatively with the IFFEFIT software package [15] by linear combination fitting (LCF) of XANES spectra [16] with spectra of reference compounds (PdS, PdO and reduced Pd nanoparticles in the range 24 345 – 24 420 eV, Fig S4a; PtO_2 and metallic Pt in the range 11 545 – 11 605 eV, Fig. S4b). During LCF the

normalized XANES spectrum of a mixture of species is fitted to a theoretical curve calculated as a linear combination of normalized reference compound spectra. The weights of the reference spectra correspond to fractions of pure species in the mixture. The highest contribution to error bars is not the statistical error (typically below $\pm$ 3%) but the phase purity of the used reference compounds which leads to a generous estimation of the uncertainty in the LCF results as $\pm$ 10% [17].

3   Results and discussion

3.1   Catalyst characterization

The as-prepared catalysts has a BET-surface area of 170 m^2/g for Pd-Pt/Al_2O_3 and 75 m²/g for Pd-Pt/CZ respectively, which is equal to the values of the pure support materials. With a narrow particle size distribution (Fig. S2) and a mean particle diameter of 4.5 nm for Pd-Pt/Al_2O_3 and 5.3 nm for Pd-Pt/CZ respectively, both catalyst show well-dispersed particles in the HAADF STEM images depicted in Fig. 1. EDXS elemental mapping confirms a composition of approximately 90 % Pd and 10 % Pt and points to formation of a homogeneous Pd-Pt alloy in the fresh catalyst samples. However, whereas on Al_2O_3 Pt is only present as alloyed particles, on CeO_2-ZrO_2-Y_2O_3-La_2O_3 Pt was also found as monometallic highly dispersed species ($<$ 1 nm). This could be due to the incipient wetness impregnation preparation method applied in this study or caused by the well-known strong interaction of Pt and ceria [18]. Both aspects would need to be investigated in the future. More advanced preparation techniques such as colloidal methods or flame spray pyrolysis, for instance, might result in particles with the two metals in closer contact. This might be especially important for CeO_2-containing supports, due to the well-known strong interaction with precious metals. As demonstrated by Jones et al. [19] for Pt/Al_2O_3, such an effect leads even to the transfer of the noble metal component to CeO_2 by simply treating a physical mixture in air at elevated temperatures (800 °C). This Pt-attraction of CeO_2 might be the driving force for the formation of the highly dispersed Pt species in addition to the Pt-Pd alloyed particles, as observed for the Pd-Pt/CeO_2-ZrO_2-Y_2O_3-La_2O_3 sample.

The support material, the prepared catalysts and the aged catalysts were characterized also by X-ray diffraction (Fig. S2). No PdO, Pd or Pt reflections were detected for the fresh CZ sample, which is in good accordance with the electron microscopy results, indicating a high dispersion of the noble metal or the presence of amorphous phases. After SO_2-aging at 450 °C, the reflections of the support material, especially for CZ, get broader, which might be explained by bulk sulfation or a phase change of the support material. Moreover, slight reflections at 34 °, 42 °, 54 ° and 72 ° were detected for the aged sample, which can be attributed to PdO and indicate slight particle sintering due to the aging. This is more pronounced for the Al_2O_3-based samples, where already for the fresh sample small reflexes of PdO were found. Considering the particle size determined by TEM (mean particle diameter of 4.5 nm), this might be explained by a higher crystallinity.
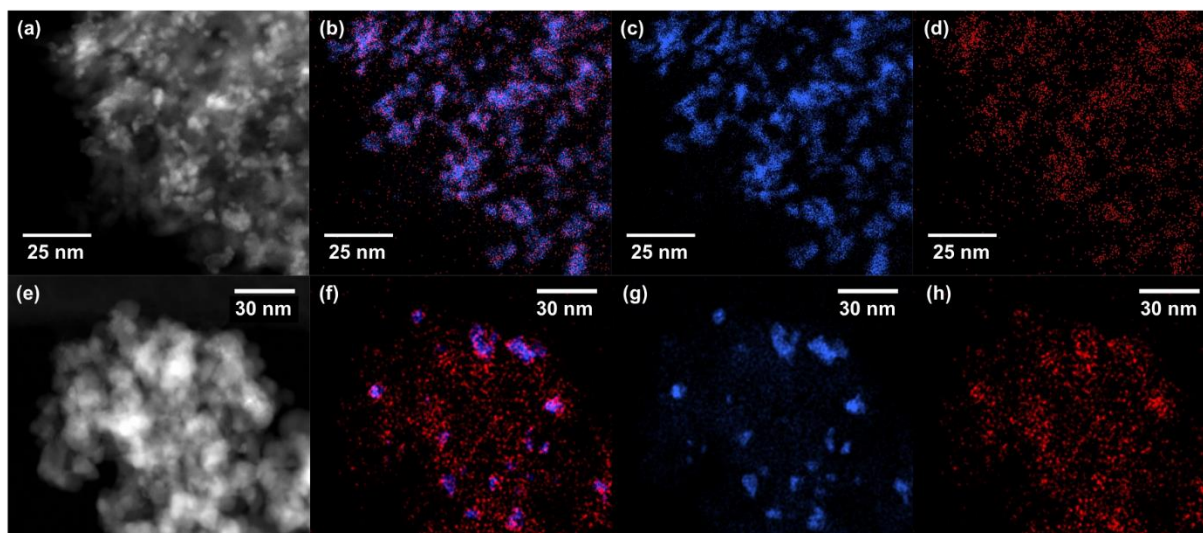
Fig. 1. HAADF STEM images (a, e) and corresponding EDXS maps (b-d, f-h) of the as-prepared (a-d) Pd-Pt/Al$_2$O$_3$ and (e-h) Pd-Pt/CZ samples. Color code: Pd L$_{\alpha 1}$-line, blue; Pt L$_{\alpha 1}$-line, red.

3.2   Laboratory catalyst tests

When comparing the initial activity in the reaction gas mixture of 3200 ppm CH$_4$, 10 % O$_2$ and 12 % H$_2$O and 5 ppm SO$_2$ in N$_2$, Pd-Pt/Al$_2$O$_3$ shows full conversion in the beginning, but loses 75 % of its activity after only 5 h of poisoning at 450 °C (Fig. S4). Pd-Pt/CZ, on the other hand, has an initial activity of 95 % methane conversion, which is maintained at 75 % after 5 h exposure to SO$_2$. This points out a slower deactivation of the ceria-zirconia supported sample. Such an effect could be due to the oxidation of some SO$_2$ at the Pt sites [20], present as monometallic nanoparticles not in the close vicinity of Pd (according to the HAADF-STEM images in Fig. 1), with storage as bulk support sulfates/sulfites, which probably additionally delays the poisoning of the Pd active sites. However, while Pd-Pt/Al$_2$O$_3$ retains some activity after the poisoning, reaching an activity plateau after approx. 10 h exposure to SO$_2$-containing atmosphere (at ~ 7 % conversion), the activity of Pd-Pt/CZ decreases further, resulting in a total loss of activity. The significant drop of activity in the presence of SO$_2$ is a well-known effect [21]. Pd-based catalysts suffer from PdSO$_4$-formation, which is inactive for methane oxidation. As already mentioned, with rising temperature SO$_2$ is oxidized to SO$_3$ over the noble metal sites, namely Pt, and finally, H$_2$SO$_4$ is formed in the presence of H$_2$O [20]. As a consequence, surface or bulk sulfates/ sulfites are formed at the noble metal sites or with the support. Support materials such as Al$_2$O$_3$ and CeO$_2$-ZrO$_2$ are able to delay the noble metal poisoning to some extent, as they can store the resulting sulfur species in the form of bulk sulfates, e.g. as Al$_2$(SO$_4$)$_3$ or Ce$_2$(SO$_4$)$_3$ [21, 22]. These species are stable up to high temperatures (approx. 700 °C) under oxygen rich or stoichiometric conditions, but can be decomposed at lower temperatures under reducing conditions [21, 23-25]. Especially for CeO$_2$ it is reported, that the sulfur remains on the support even during lean-rich cycles, forming Ce$_2$(SO$_4$)$_3$ in oxidizing conditions [23, 26]. Under reducing conditions at 400 °C, Ce$_2$O$_2$S was claimed to be formed, which reoxidzed to the sulfate again [26]. Although the addition of ZrO$_2$ to the CeO$_2$-lattice was reported to decrease the temperature of sulfates decomposition [27], deactivation occurs nevertheless, slower but even more severe for the Pd-Pt/CZ catalyst compared to the sample supported on Al$_2$O$_3$.

In the presence of NO$_x$ the deactivation process follows a similar trend for the Pd-Pt/CZ sample, with complete deactivation after about 13 h SO$_2$ exposure. In contrast, for Pd-Pt/Al$_2$O$_3$ the deactivation is significantly slowed down, as recently reported also by Sadokhina et al. [28]. Moreover, the final state shows about 15 % higher

CH$_4$ conversion in comparison to the catalyst poisoned in the absence of NO$_x$. On the one hand, this effect could be due to the positive contribution of NO$_x$ on CH$_4$ conversion over Pd-Pt/Al$_2$O$_3$ catalysts [28], which is also known do decelerate the H$_2$O deactivation process [29, 30]. On the other hand, considering that in both cases irrespective of the NO$_x$ presence the SO$_2$-exposure led to complete saturation of the catalysts (after approx.10 h for Pd-Pt/Al$_2$O$_3$ and after 13 h for Pd-Pt/CZ), the remaining activity shown by the alumina supported sample is possibly more related to the final state of the noble metal components. As indicated by the electron microscopy measurements (Fig. 1), mainly bimetallic Pd-Pt particles were identified for the alumina sample whereas monometallic Pt is also present on the CeO$_2$-ZrO$_2$ supported catalyst. Indeed, the evolution of the NO$_2$/NO concentrations during catalyst deactivation indicates a simultaneous and complete decrease of the NO to NO$_2$ conversion for the CeO$_2$-ZrO$_2$ supported sample (Table S2). In contrast, the Pd-Pt/Al$_2$O$_3$ catalyst shows a remaining 14 % NO oxidation to NO$_2$ after 15 h catalyst poisoning. This suggests that a certain extent of the noble metal sites in the alumina supported sample is still active not only for CH$_4$ oxidation but also for the NO oxidation reaction, which is probably Pt. At the same time, the different distribution of the noble metal components on the CeO$_2$-ZrO$_2$ support, as bimetallic but also monometallic nanoparticles, seems to lead to a state more sensitive towards SO$_2$ poisoning, which is even more pronounced in the presence of NO$_x$.

To regenerate the SO$_2$-poisoned samples, a 1 h reductive treatment was applied at 500 °C or at 550 °C. The results depicted in Fig. 2 show a complete regeneration of the activity for both catalysts after poisoning in the absence of NO$_x$. Upon regeneration at 500 °C, Pd-Pt/CZ showed again a slightly slower aging process, however, ending up in 0 % conversion after 15 h. While the alumina-based sample shows the same rate of deactivation after regeneration at 500 °C or 550 °C, choosing a higher regeneration temperature results in a more decelerated activity loss for Pd-Pt/CZ. This could be explained by a more efficient removal of the support related sulfur species formed on Pd-Pt/CZ, which once again acts as a SO$_2$/SO$_3$ storage material. It should also be mentioned that Pd-Pt/Al$_2$O$_3$ still shows some activity after reaching a plateau, but this activity decreases from approx. 7 % to 3 % after the second reactivation cycle. Such a behavior could be due to a slight sintering of the noble metal particles occurring during exposure to higher temperature and reducing atmosphere for catalyst regeneration [31], but also due to a promoted sintering by SO$_2$ [32]. This assumption is supported by the XRD data, indicating the sintering of PdO particles after just 15 h of SO$_2$-aging (Fig S2) and after the aging and regeneration cycles (Fig. S5) described above and presented in Fig. 2. The increased reflexes at 34 °, 42 ° and 54 ° and 72 ° clearly point to the existence of larger PdO particles compared to the fresh catalyst sample.
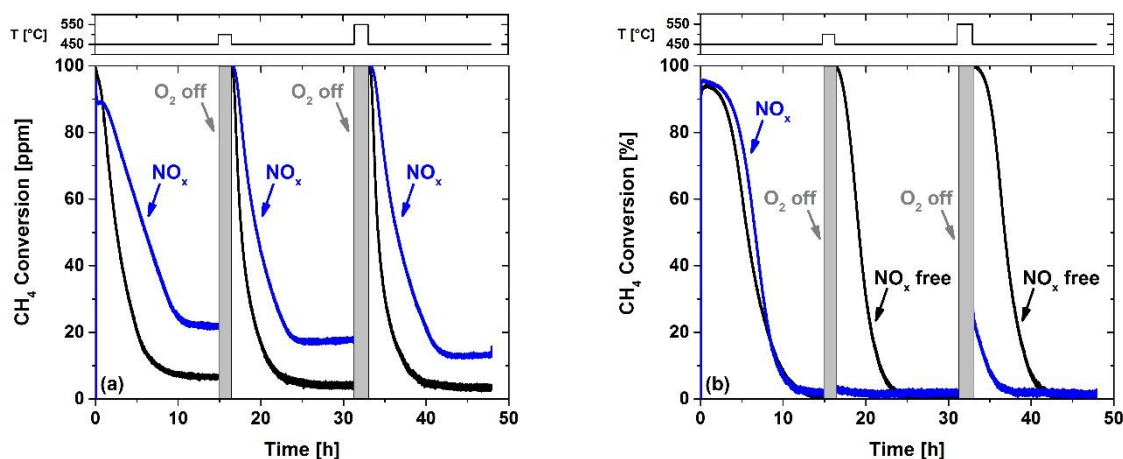

Fig. 2. CH$_4$ conversion during aging and regeneration of (a) Pd-Pt/Al$_2$O$_3$ and (b) Pd-Pt/CZ. Aging for 15 h at 450 °C in 3200 ppm CH$_4$, 10 % O$_2$, 12 % H$_2$O, 5 ppm SO$_2$ in N$_2$ (black line, GM 2) or 120 ppm NO and 30 ppm NO$_2$ (blue, GM 3) added.

Regeneration for 1 h at 500 °C (1st regeneration) and 550 °C (2nd regeneration) by turning off the oxygen (GM 4 and 5). GHSV kept constant at 80 000 h^{-1} by balancing with N$_2$.

Whereas the NO$_x$ impact is not significant during SO$_2$-poisoning of Pd-Pt/CZ, a tremendous effect is observed during catalyst regeneration. Basically, only Pd-Pt/Al$_2$O$_3$ could be regenerated by reductive treatment at 500 °C, which resulted in complete reactivation and a slightly faster catalyst re-poisoning during the second SO$_2$ exposure. On the contrary, Pd-Pt/CZ shows no significant activity after the reductive treatment, a further increase of the regeneration temperature to 550 °C results only in partial reactivation. Again, this behavior is probably due to the different state of the noble metals on the two support materials.

3.3   *Operando* XAS during aging and regeneration

To elucidate the differences appearing in the aging and regeneration behavior of the ceria-zirconia and alumina catalysts, *ex situ* and *operando* XAS measurements were performed under reaction conditions similar to those applied during the lab bench tests while monitoring the state of Pd and Pt. Since, based on the results from the lab tests, these were considered to be the most relevant conditions for real applications, the catalyst samples were exposed to 3200 ppm CH$_4$, 10 % O$_2$, 12 % H$_2$O, 30 ppm SO$_2$, 150 ppm NO and 50 ppm NO$_2$ in N$_2$ at 450 °C for one hour. In contrast to the laboratory tests, the poisoning temperature of 450 °C was also used for catalyst regeneration to be able to capture the transient state of the noble metal during switching to the reducing conditions. As the results of the linear combination analysis of the XANES region indicate, the palladium is exclusively present as PdO in the fresh Pd-Pt/Al$_2$O$_3$ catalyst, which is in line with one of our previous studies [29], and no bulk PdSO$_4$ formation was observed during the 1 h aging with SO$_2$ (Fig. 3a). However, the activity data showed a clear drop during poisoning (Fig. S9), which could be explained by a partial poisoning of Pd-Pt particles (e.g. on the surface). When oxygen was turned off during the regeneration step (t = 0 s on the X scale in Fig. 3a), changes of the Pd phase are visible, consisting in appearance of metallic Pd and of PdS. This goes along with a pronounced SO$_2$ desorption (Fig. S8). At the end of the regeneration step the species observed amounted to approximately 45 % PdS and 65 % metallic Pd. Hence, when developing regeneration strategies for MOCs, the formation of PdS, which is inactive for methane oxidation, needs to be considered. Returning to the lean conditions of methane oxidation reaction mixture results in an immediate conversion of PdS to PdO (Fig. 3b). Approximately 80 % PdO and 20 % of Pd were observed after 3 min in lean atmosphere. However, at this temperature full re-oxidation appears to be a slower process taking up to 20 min, as can be seen in Fig. 3b. At the same time, the Pt L$_3$-XAS data show that 60 % of the Pt are in oxidized state in lean atmosphere and almost completely reduced Pt species are formed during the rich period (Fig. S7a). Re-oxidation in oxygen-containing atmosphere occurs up to 50 % (Fig. S7b). The lack in catalyst response when turning oxygen off or on is caused by the XAS experiment parameters. There is a dead volume given by the gas lines and the capillary reactor leading to delayed response, but more important, the much higher concentration of oxygen of 10 % in comparison to only 3200 ppm CH$_4$ will also cause some delay. On the other side, we measured at mid position of the catalyst bed with a small beam (400 x 260 µm). Therefore, as soon as the oxygen concentration decreases, the beginning of the catalyst bed will be affected at first, followed by the mid and the end of the catalyst bed.

For Pd-Pt/CZ, on the other hand, no changes in oxidation state were observed when varying the gas composition, exclusively PdO was detected and no regeneration of the catalyst was noticed. This behavior is in agreement with the activity data obtained during the *operando* experiment (Fig. S8) and the lab bench activity tests presented above. This different response of the two catalysts in the presence or absence of NO$_x$ is clearly related

to the ability of some of the noble metal sites present on alumina to activate the CH_4 molecule for reducing sulfur species formed at Pd sites already at 450 °C. Considering the complete loss of activity for CH_4 and NO oxidation of the Pd-Pt/CZ sample upon SO_2 poisoning at 450 °C, the reduction of the poisoned noble metal sites and the regeneration of this catalyst seems to be possible only at higher temperature, i.e. above 550 °C.
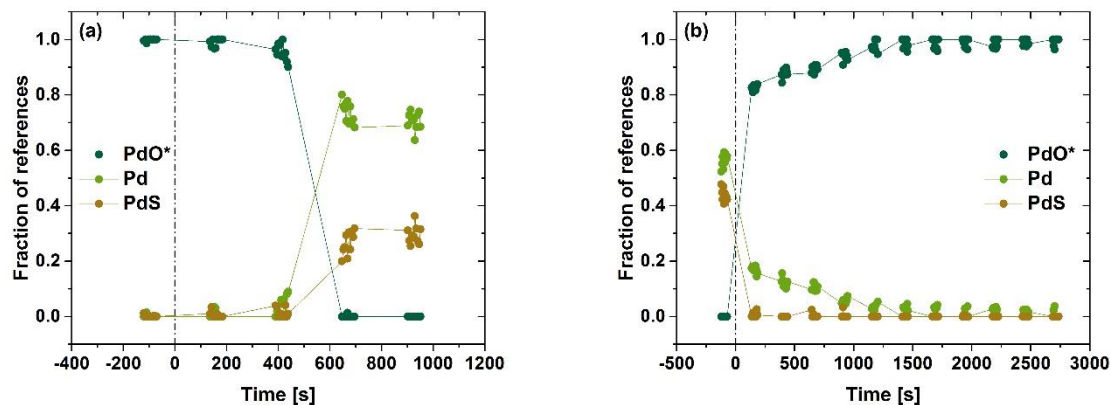

Fig. 3. Pd species on Pd-Pt/Al_2O_3 during (a) regeneration in oxygen-free conditions and (b) reaction mixture after regeneration based on linear combination fitting of PdO, Pd and PdS reference spectra. Conditions: 3200 ppm CH_4, 0/10 % O_2, 12 % H_2O, 150 ppm NO, 50 ppm NO_2, 30 ppm SO_2 in N_2, T = 450 °C. GHSV = 500 000 h^{-1}. Changes in gas composition always at t = 0. *PdO is poisoned by surface sulfites and sulfates after the sulfur poisoning according to activity data, which are, however, not visible in the XAS spectra. Hence, PdO was used for LCF.

4   Conclusions

SO_2 aging and subsequent regeneration in rich conditions were studied under NO_x-free and NO_x-containing gas atmosphere for Pd-Pt catalysts supported on Al_2O_3 and CeO_2-ZrO_2. It was found, that the deactivation process at 450 °C is slower during the first hours for Pd-Pt/CZ compared to Pd-Pt/Al_2O_3. However, poisoning is more severe after 15 h on stream since no activity remains, whereas Pd-Pt/Al_2O_3 perpetuates 7 % methane conversion. In the absence of NO_x, the efficiency of regeneration in oxygen-free gas mixtures increases at higher temperatures and is more sustainable for Pd-Pt/CZ.

Addition of NO_x leads to a decelerated aging process for both catalyst systems, preserving a higher methane oxidation activity for the alumina supported sample in comparison to the NO_x-free conditions. However, a complete deactivation was recorded for Pd-Pt/CZ under these conditions. The effect of NO_x presence and especially of the carrier material was even more pronounced during the regeneration step. Similar to the NO_x-free conditions, Pd-Pt/Al_2O_3 was completely reactivated already at 500°C. On the contrary, Pd-Pt/CZ could be only slightly regenerated at 550°C. *Operando* XAS unraveled the regeneration of the sulfur poisoned Pd-Pt/Al_2O_3 catalysts via PdS and Pd formation during the rich treatment. Both species are converted to PdO when switching back to the reaction mixture, resulting in recovery of the catalytic activity. Due to a different distribution of the noble metal components on the ceria-zirconia supported catalyst used in this study, which includes monometallic Pt nanoparticles, the reduction of the sulfated Pd-sites and catalyst regeneration in the presence of NO_x seems to be possible only at higher temperatures (> 500 °C).

By combining systematic lab-bench tests and advanced *operando* XAS techniques, important aspects of the sulfur poisoning and regeneration of MOCs were uncovered. It was demonstrated that poisoning and regeneration strategies developed and observed for model-like reaction conditions might not be easily transferable to applied

conditions, especially for different catalyst formulations. In this regard, the role of the support material seems to be mandatory during aging and regeneration of Pd-Pt MOCs. All these facets require further investigations, including catalyst testing under more complex reaction mixtures, advanced preparation methods and *operando* characterization.

Acknowledgements

Supplementary data

Supplementary data associated with this article can be found in the online version at Link to webpage.

References

[1]   P. Gelin, M. Primet, Appl. Catal. B 39 (2002) 1-37.

[2]   O. Deutschmann, J.-D. Grunwaldt, Chem. Ing. Tech. 85 (2013) 595-617.

[3]   G. Lapisardi, L. Urfels, P. Gelin, M. Primet, A. Kaddouri, E. Garbowski, S. Toppi, E. Tena, Catal. Today 117 (2006) 564-568.

[4]   D. Ciuparu, L. Pfefferle, Appl. Catal. A 209 (2001) 415-428.

[5]   J.K. Lampert, M.S. Kazi, R.J. Farrauto, SAE Technical Paper 961971 (1996).

[6]   M.S. Wilburn, W.S. Epling, Appl. Catal. B 206 (2017) 589-598.

[7]   D.L. Mowery, M.S. Graboski, T.R. Ohno, R.L. McCormick, Appl. Catal. B 21 (1999) 157-169.

[8]   T. Hamzehlouyan, C.S. Sampara, J.H. Li, A. Kumar, W.S. Epling, Appl. Catal. B 181 (2016) 587-598.

[9]   K. Narui, H. Yata, K. Furuta, A. Nishida, Y. Kohtoku, T. Matsuzaki, Appl. Catal. A 179 (1999) 165-173.

[10]   F. Arosio, S. Colussi, G. Groppi, A. Trovarelli, Catal. Today 117 (2006) 569-576.

[11]   M. Honkanen, J. Wang, M. Kärkkäinen, M. Huuhtanen, H. Jiang, K. Kallinen, R.L. Keiski, J. Akola, V. Minnamari, J. Catal. 358 (2018) 253-256.

[12]   A. Gremminger, P. Lott, M. Merts, M. Casapu, J.-D. Grunwaldt, O. Deutschmann, Appl. Catal. B 218 (2017) 833-843.

[13]   W. Kleist, J.-D. Grunwaldt, High Output Catalyst Development in Heterogeneous Gas Phase Catalysis, in: A. Hagemeyer, A.F. Volpe, (Eds.), Modern Applications of High Throughput R&D in Heterogeneous Catalysis, Bentham Science Publishers 2014, pp. 357-371.

[14]   J.-D. Grunwaldt, N. van Vegten, A. Baiker, Chem. Commun. (2007) 4635-4637.

[15]   B. Ravel, M. Newville, J. Synchrotron Radiat. 12 (2005) 537-541.

[16]   M. Benfatto, C. Meneghini, A Close Look into the Low Energy Region of the XAS Spectra: The XANES Region, in: S. Mobilio, F. Boscherini, C. Meneghini, (Eds.), Synchrotron Radiation, Springer, Berlin, Heidelberg, 2015, pp. 213-240.

[17]   S.D. Kelly, K.M. Kemner, J.B. Fein, D.A. Fowle, M.I. Boyanov, B.A. Bunker, N. Yee, Geochim. Cosmochim. Acta 66 (2002) 3855-3871.

[18] A.M. Gänzler, M. Casapu, P. Vernoux, S. Loridant, F.J.C.S. Aires, T. Epicier, B. Betz, R. Hoyer, J.-D. Grunwaldt, Angew. Chem., Int. Ed. 56 (2017) 13078-13082.

[19] J. Jones, H.F. Xiong, A.T. Delariva, E.J. Peterson, H. Pham, S.R. Challa, G.S. Qi, S. Oh, M.H. Wiebenga, X.I.P. Hernandez, Y. Wang, A.K. Datye, Science 353 (2016) 150-154.

[20] T. Hamzehlouyan, C. Sampara, J.N. Li, A. Kumar, W. Epling, Top. Catal. 59 (2016) 1028-1032.

[21] J.K. Lampert, M.S. Kazi, R.J. Farrauto, Appl. Catal. B 14 (1997) 211-223.

[22] S. Colussi, F. Arosio, T. Montanari, G. Busca, G. Groppi, A. Trovarelli, Catal. Today 155 (2010) 59-65.

[23] T. Luo, R.J. Gorte, Appl. Catal. B 53 (2004) 77-85.

[24] D.W. Kwon, K.B. Nam, S.C. Hong, Appl. Catal. B 166 (2015) 37-44.

[25] T.J. Truex, SAE Technical Paper 961971 (1999).

[26] T. Luo, J.M. Vohs, R.J. Gorte, J. Catal. 210 (2002) 397-404.

[27] P. Bazin, O. Saur, J.C. Lavalley, A.M. Le Govic, G. Blanchard, Stud. Surf. Sci. Catal. 116 (1998) 571-579.

[28] N. Sadokhina, G. Smedler, U. Nylen, M. Olofsson, L. Olsson, Appl. Catal. B 236 (2018) 384-395.

[29] A.T. Gremminger, H.W.P. de Carvalho, R. Popescu, J.-D. Grunwaldt, O. Deutschmann, Catal. Today 258 (2015) 470-480.

[30] N. Sadokhina, G. Smedler, U. Nylen, M. Olofsson, L. Olsson, Appl. Catal. B 200 (2017) 351-360.

[31] J.M. Jones, V.A. Dupont, R. Brydson, D.J. Fullerton, N.S. Nasri, A.B. Ross, A.V.K. Westwood, Catal. Today 81 (2003) 589-601.

[32] X. Auvray, T. Pingel, E. Olsson, L. Olsson, Appl. Catal. B 129 (2013) 517-527.